

THE ATMOSPHERIC DYNAMICS OF AGB STARS REVEALED BY GAIA THROUGH NUMERICAL SIMULATIONS

A. Chiavassa¹, B. Freytag² and M. Schultheis¹

Abstract.

A considerable fraction of the detected intrinsically variable stars in Gaia data are Long-Period Variables. These objects have large luminosity amplitudes and variability timescales. They have complex stellar surface dynamics that affect the measurements and amplify the uncertainties on stellar parameters.

We explore the impact of the convection-related surface structure in AGBs on the photocentric variability. We quantify these effects to characterise the observed parallax errors and estimate fundamental stellar parameters and dynamical properties.

For this purpose, we use state-of-the-art three-dimensional (3D) radiative hydrodynamics simulations of convection with CO5BOLD and the post-processing radiative transfer code OPTIM3D to compute intensity maps in the Gaia G band [325 – 1030 nm]. Then, we calculate the intensity-weighted mean of all emitting points tiling the visible stellar surface (i.e. the photocentre) and evaluate its motion as a function of time. We show that the convection-related variability accounts for a substantial part of the Gaia DR2 parallax error of our sample of semi-regular variables. We prospect the roadmap to extract quantitatively fundamental properties of AGB stars directly from Gaia errors exploiting appropriate RHD simulations.

Keywords: stars: atmospheres, stars: AGB and post-AGB, astrometry, parallaxes

1 Introduction

Gaia (Gaia Collaboration et al. 2016) is an astrometric, photometric, and spectroscopic space-borne mission. It performs a survey of a large part of the Milky Way. The second data release (Gaia DR2 Gaia Collaboration et al. 2018) brought high-precision astrometric parameters (i.e. positions, parallaxes, and proper motions) for over 1 billion sources brighter than $G \approx 20$. The time resolution of the Gaia measurements allows the classification and detailed study of an unmatched number of variable objects. A considerable fraction of the detected intrinsically variable stars are Long-Period Variables (LPVs), that have large luminosity amplitudes and variability timescales that are covered adequately by Gaia (Gaia Collaboration et al. 2019). Recently, Holl et al. (2018) found 151 761 LPV candidates that fulfil these characteristics.

LPVs are cool luminous evolved stars which reached a critical phase of their evolution and increased the mass-loss ejections. They are characterised: (i) by large-amplitude variations in radius, brightness, and temperature of the star; and (ii) by a strong mass-loss rate driven by an interplay between pulsation, dust formation in the extended atmosphere, and radiation pressure on the dust (Höfner & Olofsson 2018). LPVs eject a significant fraction of their mass by stellar winds contributing extensively to the cosmic matter cycle. They provide substantial amounts of chemically enriched gas and dust grains to the interstellar medium, and thereby to new generations of stars and planets.

The surface of the deep convection zone of those objects are characterised by large and small convective cells. The visible fluffy stellar surface is made of shock waves that are produced in the interior and are shaped by the top of the convection zone as they travel outward (Freytag et al. 2017). In addition to this, in the optical thin region and on the top of the convection-related surface structures (i.e. further up in the atmosphere with respect to the continuum-forming region) also the opacity affects the observable domain. In particular at the wavelengths in Gaia G-band (Evans et al. 2018), where TiO molecules produce strong absorptions. All these

¹ Université Côte d'Azur, Observatoire de la Côte d'Azur, CNRS, Lagrange, CS 34229, Nice, France

² Department of Physics and Astronomy at Uppsala University, Regementsvägen 1, Box 516, SE-75120 Uppsala, Sweden

effects alter the position of the photocentre and cause temporal fluctuations during the Gaia mission, as already pointed out for red supergiant stars in Chiavassa et al. (2011).

In this work, we explore the impact of the variability of the stellar surface granulation-related structures on Gaia parallax determination and explore the possibility to extract stellar properties, such as the fundamental stellar parameters, may be hidden behind the Gaia measurement uncertainty.

2 Observation sample

First we selected a sample of semiregular variables from different catalogues (Tabur et al. 2009; Glass & van Leeuwen 2007; Jura et al. 1993) with luminosities ($4000 < L_{\odot} < 8000$) matching the theoretical luminosities from RHD simulations introduced in next section. Then, we extracted the corresponding parallax error (σ_{ϖ}) from Gaia DR2. More details about the cross-identification with the distance catalogue of Bailer-Jones et al. (2018) are reported in Chiavassa et al. (2018). Ultimately, it has to be noted that σ_{ϖ} may still vary in the following data releases because: (i) the mean number of measurements for each source amounts to 26 (Mowlavi et al. 2018) and this number will be 70-80 in total at the end of the nominal mission; (ii) and new solutions may be applied to adjust the imperfect chromaticity correction (Arenou et al. 2018).

3 Gaia measurements decrypted with numerical simulations

3.1 Methods

We aim at obtaining intensity maps in the Gaia G photometric system (Evans et al. 2018) combining the thermodynamic structures of the outer layers of the atmosphere AGB stars with detailed radiative transfer calculation.

For this purpose, we used the radiation-hydrodynamics (RHD) simulations of AGB stars (Freytag et al. 2017) computed with the CO5BOLD code (Freytag et al. 2012). The code solves the coupled non-linear equations of compressible hydrodynamics and non-local radiative energy transfer in the presence of a fixed external spherically symmetric gravitational field in a three-dimensional (3D) cartesian grid. It is assumed that solar abundances are appropriate for M-type AGB stars. The basic stellar parameters of the RHD simulations are reported in Table 1. In the simulations, convection, waves, and shocks all contribute to the dynamical pressure and, therefore, to an increase of the stellar radius and to a levitation of material into layers where dust can form. No dust is included in any of these simulations. The regularity of the pulsations decreases with decreasing gravity as the relative size of convection cells increases. The pulsation period is extracted with a fit of the Gaussian distribution in the power spectra of the simulations. The period of the dominant mode increase with the radius of the simulation (Freytag et al. 2017).

Then, we employed the code OPTIM3D (Chiavassa et al. 2009), which takes into account the Doppler shifts caused by the convective motions, to compute intensity maps based on snapshots from the RHD simulations of Table 1. The code uses pre-tabulated extinction coefficients per unit mass (same as in Gustafsson et al. 2008) as a function of temperature, density, and wavelength for the solar composition (Asplund et al. 2009). Micro-turbulence broadening is set to zero.

Table 1. RHD simulation parameters.

Simulation	M_{\star} [M_{\odot}]	L_{\star} [L_{\odot}]	R_{\star} [AU]	T_{eff} [K]	$\log g$ [cgs]	t_{avg} [yr]	P_{puls} [yr]	σ_{puls} [yr]	$\langle P \rangle$ [AU]	σ_P [AU]
st26gm07n002	1.0	6986	2.04	2524	-0.85	25.35	1.625	0.307	0.262	0.187
st26gm07n001	1.0	6953	1.87	2635	-0.77	27.74	1.416	0.256	0.275	0.198
st28gm06n26	1.0	6955	1.73	2737	-0.70	25.35	1.290	0.317	0.241	0.152
st29gm06n001	1.0	6948	1.62	2822	-0.65	25.35	1.150	0.314	0.266	0.174
st27gm06n001	1.0	4982	1.61	2610	-0.64	28.53	1.230	0.088	0.150	0.101
st28gm05n002	1.0	4978	1.46	2742	-0.56	25.35	1.077	0.104	0.133	0.077
st28gm05n001	1.0	4990	1.40	2798	-0.52	25.36	1.026	0.135	0.183	0.131
st29gm04n001	1.0	4982	1.37	2827	-0.50	25.35	0.927	0.100	0.152	0.078

The table shows the simulation name, the mass M_{\star} , then several time-averaged quantities: emitted luminosity L_{\star} , stellar radius R_{\star} , effective temperature T_{eff} , surface gravity $\log g$, pulsation period P_{puls} , the half of the distribution of the pulsation frequencies σ_{puls} , and the stellar time t_{avg} used for the averaging. All these quantities are from Freytag et al. (2017). The last two columns are the time-averaged value of the photocentre displacement ($\langle P \rangle$) and its standard deviation (σ_P), as in Chiavassa et al. (2018).

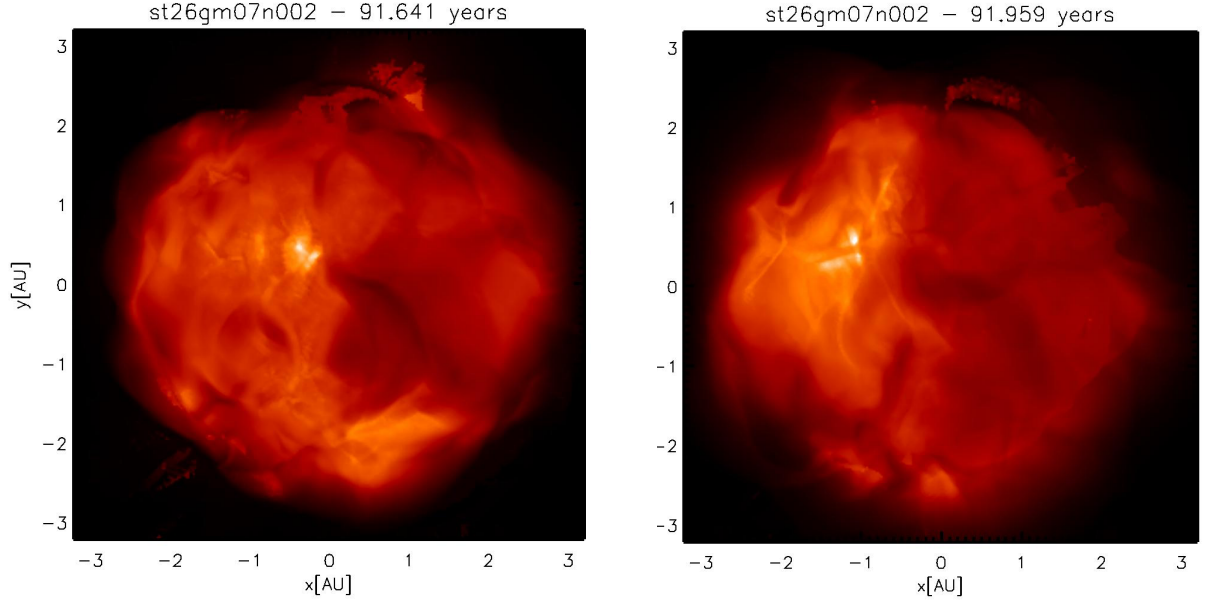


Fig. 1. Example of the squared root intensity maps (the range is $[0, -\sqrt{3000}]$ erg/s/cm²/Å) in the Gaia *G* photometric system (from 325 to 1030 nm, Evans et al. 2018) for two different snapshots of one simulation listed in Table 1. The number on the top indicates the stellar times at which the two snapshots were computed. This figure is similar to Fig. 1 of Chiavassa et al. (2018) but for another simulation.

3.2 Comparison with observations

In the Gaia *G* photometric system, few large surface structures with sizes of a third of the stellar radii (≈ 0.6 AU) are visible (Fig. 1). They evolve on a temporal scale of several months to a few years, as well as a few short-lived (weeks to month) convective cells at smaller scales ($< 10\%$ of the stellar radius).

We calculated the position of the photocentre for each map (i.e. as a function of time) as the intensity-weighted mean of the $x - y$ positions of all emitting points tiling the visible stellar surface according to

$$P_x = \frac{\sum_{i=1}^N \sum_{j=1}^N I(i, j) * x(i, j)}{\sum_{i=1}^N \sum_{j=1}^N I(i, j)} \quad (3.1)$$

$$P_y = \frac{\sum_{i=1}^N \sum_{j=1}^N I(i, j) * y(i, j)}{\sum_{i=1}^N \sum_{j=1}^N I(i, j)}, \quad (3.2)$$

where $I(i, j)$ is the emerging intensity for the grid point (i, j) with coordinates $x(i, j)$, $y(i, j)$ of the simulation, and $N = 281$ is the total number of grid points in the simulated box. In the presence of surface brightness asymmetries, the photocentre position does not coincide with the barycentre of the star and its position change as the surface pattern changes with time. The time-averaged photocentre position ($\langle P \rangle$) and its standard deviations (σ_P) are reported in Table 1 for all the RHD simulations. Depending on the simulation, σ_P varies between 0.077 and 0.198 AU (≈ 5 to $\approx 11\%$ of the corresponding stellar radius, Chiavassa et al. 2018). The value of σ_P is mostly fixed by the short time scales corresponding to the small atmospheric structures and it is increasing with lower surface gravity (Fig. 2).

Fig. 3 (left panel) displays Gaia parallax errors against the luminosity and compares these results to the standard deviations of the photocentre displacement in the simulations from Table 1. The latter show good agreement with the observations. This attests that convection-related variability accounts for a substantial part of the parallax error in Gaia measurements (Chiavassa et al. 2018). However, the observed and simulated luminosities do not coincide exactly and the observed error bars are still very large. One limitation of the

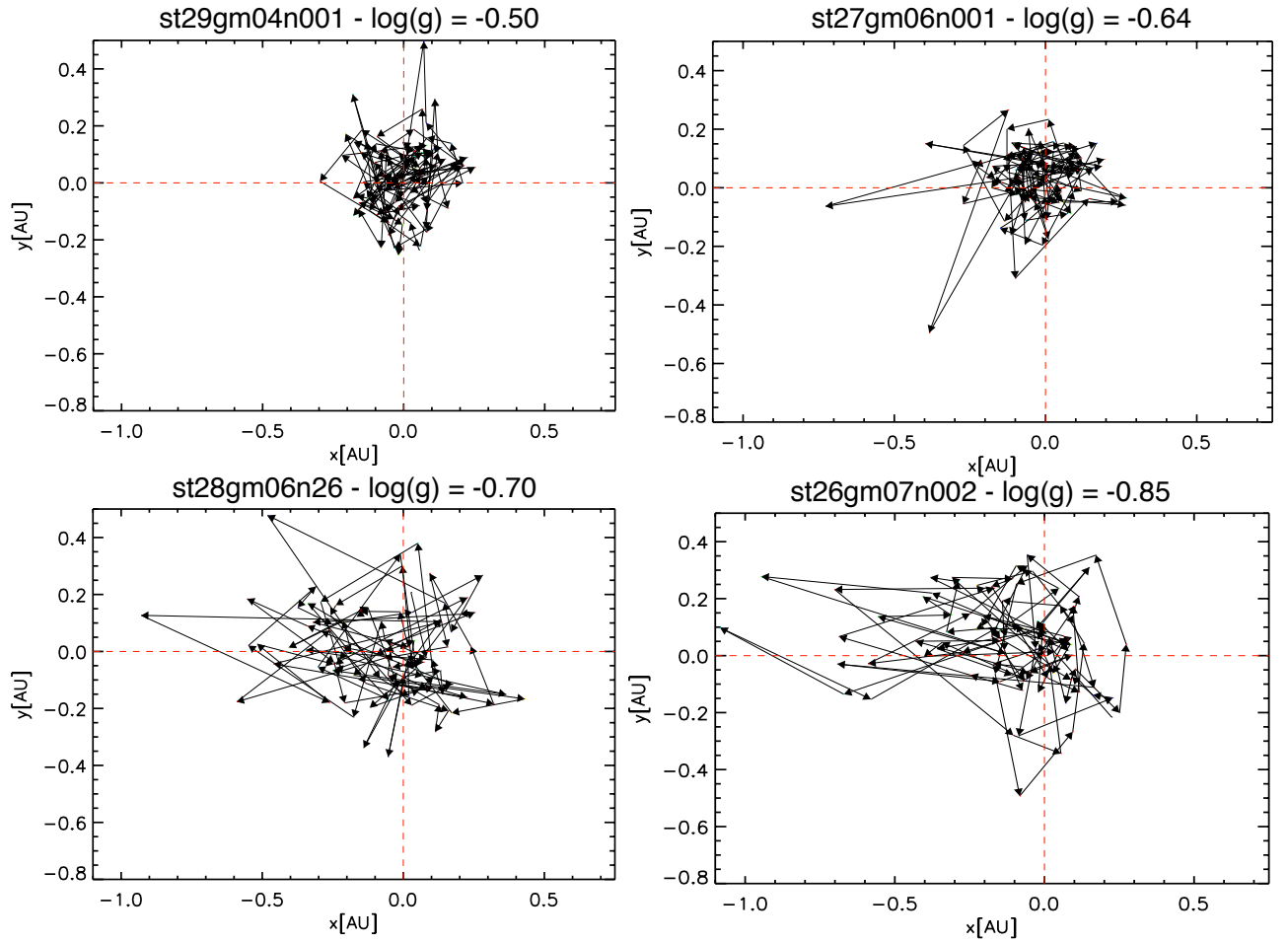


Fig. 2. Photocentre positions computed from four different RHD simulations of Table 1 in the Gaia G band filter. The different snapshots are connected by the line segments; the total time covered is reported in the Table. The dashed lines intersect at the position of the geometrical centre of the images.

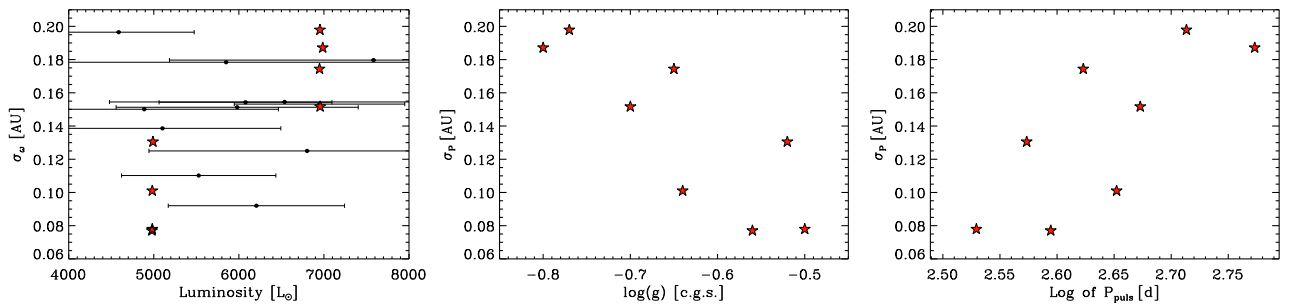


Fig. 3. *Left panel:* Luminosity against the parallax error of the observations (σ_w , circle symbol in black) and the standard deviation of the photocentre displacement for the RHD simulations of Table 1 (σ_P , star symbol in red). *Central panel:* σ_P against the surface gravity for the RHD simulations. *Right panel:* σ_P against the logarithm of the period. This figure is from Chiavassa et al. (2018).

existing model grid is the restriction to $1 M_{\odot}$. In the future, there will be models with other masses available.

Using the stellar parameters extracted from RHD simulations (Table 1), Chiavassa et al. (2018) denoted a correlation between the mean photocentre displacement and those quantities as plotted in Fig. 3. The central panel displays that lower surface gravity (i.e. more extended atmospheres) causes larger excursions of the

photocentre. This behaviour is explained by the correlation between the stellar atmospheric pressure scale height ($H_p \approx \frac{T_{\text{eff}}}{g}$) and the photocentre displacement (Freytag 2001; Ludwig 2006; Chiavassa et al. 2011). Larger values of σ_P correspond to longer pulsation periods (Fig. 3, right panel). This result is likely associated with the P-L relation found by Freytag et al. (2017), who showed that the periods in RHD simulations are consistent with observed periods of Whitelock et al. (2009).

Given the fact that σ_P explains Gaia measurement uncertainties on the parallaxes, we suggest that parallax variations from Gaia measurements could be exploited quantitatively using appropriate RHD simulations to extract, in a unique way, the fundamental properties of AGB stars such as the surface gravity and the pulsation periods. The first governs the size of granules that, in turn, controls the photometric variations. The second gives important information about stellar (mean) interior with information about global shocks induced by large-amplitude, radial, and fundamental-mode pulsations.

4 Conclusions and future perspectives within the next Gaia Data Releases

We used the snapshots from RHD simulations of AGB stars with different stellar parameters to compute intensity maps in the Gaia G photometric system. We found that the stellar dynamics in the simulations induce an intrinsic noise to the measurement uncertainty on the parallax of a sample of AGB stars in the solar neighbourhood and cross-matched with data from the Gaia DR2. The good agreement in the comparisons suggests that convection-related variability accounts for a substantial part of the parallax error, as already pointed out in Chiavassa et al. (2018). Moreover, an important piece of information is indeed hidden in the Gaia measurement uncertainty. The fundamental properties of AGB stars could be measured directly from Gaia parallax and photometric errors exploiting quantitatively appropriate RHD simulations.

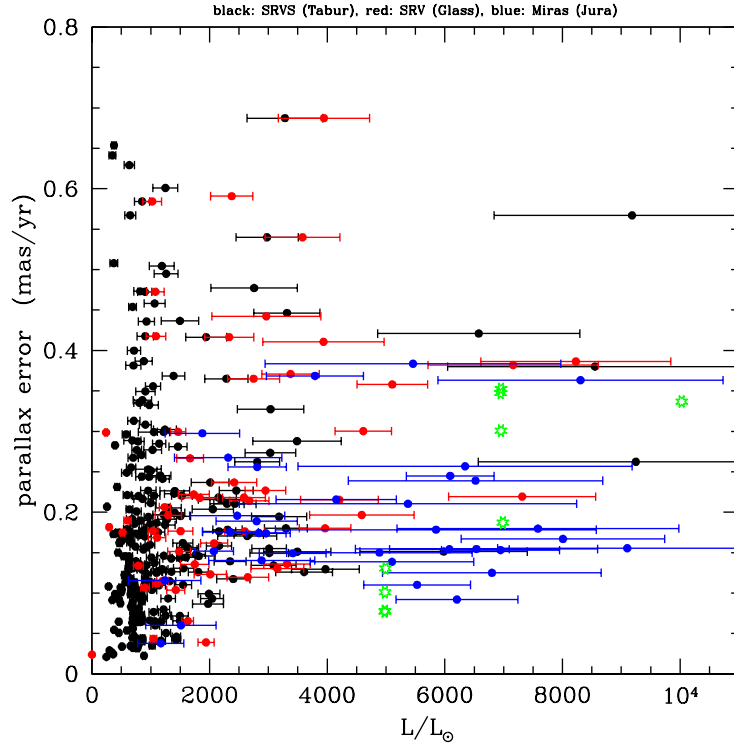


Fig. 4. Parallax error from Gaia DR2 as a function of their luminosity for a sample of semiregular variables from (Tabur et al. 2009, black), (Glass & van Leeuwen 2007, red), and (Jura et al. 1993, blue) marked with different colors. The light green stars denote the position of the RHD simulations from Table 1.

This requires a series of steps that we list here for the next years:

- Study of the photometric Radial Velocity predicted signatures from current RHD simulations grid. Chiavassa et al. (2011) showed that massive evolved red supergiant stars, with close enough stellar parameters

to AGBs, have magnitude excursion up to 0.28 and 0.13 magnitudes in the blue and red Gaia photometric filters, respectively, with a strong impact on the parameter determination. We expected similar (or higher) values for AGBs.

- Significantly larger RHD simulation grid (at least 5 times more simulations with respect to the actual grid) is necessary to explore a large number of AGBs in Gaia. Fig. 4 displays a larger sample of variables from different catalogues for which Gaia DR2 data have provided measurements. Today RHD simulations (light green stars) cover only a small region of the parameter space.
- With Gaia DR2, the mean number of measurements for each source amounts to ≈ 26 (Mowlavi et al. 2018). Eventually, when Gaia DR4 will be available in 2022, the number of measurements will increase to 70-80, and possibly reducing the parallax error. In addition to this, also the temporal variation of the photometric and astrometric measurements will be available making conceivable a direct and more precise comparison with the time-dependent RHD simulations.

In the end, combining our unique global 3D simulations with Gaia data will make it possible to systematically study the properties of convection in stars other than the sun.

This work has made use of data from the European Space Agency (ESA) mission Gaia (<https://www.cosmos.esa.int/gaia>), processed by the Gaia Data Processing and Analysis Consortium (DPAC, <https://www.cosmos.esa.int/web/>). Funding for the DPAC has been provided by national institutions, in particular the institutions participating in the Gaia Multilateral Agreement. This work has been supported by the Swedish Research Council (Vetenskapsrådet). The computations were performed on resources (rackham) provided by SNIC through Uppsala Multidisciplinary Center for Advanced Computational Science (UPPMAX) under Projects snic2017-1-41 and snic2018-3-74.

References

- Arenou, F., Luri, X., Babusiaux, C., et al. 2018, *A&A*, 616, A17
- Asplund, M., Grevesse, N., Sauval, A. J., & Scott, P. 2009, *ARA&A*, 47, 481
- Bailer-Jones, C. A. L., Rybizki, J., Fouesneau, M., Mantelet, G., & Andrae, R. 2018, *AJ*, 156, 58
- Chiavassa, A., Freytag, B., & Schultheis, M. 2018, *A&A*, 617, L1
- Chiavassa, A., Pasquato, E., Jorissen, A., et al. 2011, *A&A*, 528, A120
- Chiavassa, A., Plez, B., Josselin, E., & Freytag, B. 2009, *A&A*, 506, 1351
- Evans, D. W., Riello, M., De Angeli, F., et al. 2018, *A&A*, 616, A4
- Freytag, B. 2001, in *Astronomical Society of the Pacific Conference Series*, Vol. 223, 11th Cambridge Workshop on Cool Stars, Stellar Systems and the Sun, ed. R. J. Garcia Lopez, R. Rebol, & M. R. Zapaterio Osorio, 785
- Freytag, B., Liljegren, S., & Höfner, S. 2017, *A&A*, 600, A137
- Freytag, B., Steffen, M., Ludwig, H. G., et al. 2012, *Journal of Computational Physics*, 231, 919
- Gaia Collaboration, Brown, A. G. A., Vallenari, A., et al. 2018, *A&A*, 616, A1
- Gaia Collaboration, Eyer, L., Rimoldini, L., et al. 2019, *A&A*, 623, A110
- Gaia Collaboration, Prusti, T., de Bruijne, J. H. J., et al. 2016, *A&A*, 595, A1
- Glass, I. S. & van Leeuwen, F. 2007, *MNRAS*, 378, 1543
- Gustafsson, B., Edvardsson, B., Eriksson, K., et al. 2008, *A&A*, 486, 951
- Höfner, S. & Olofsson, H. 2018, *A&A Rev.*, 26, 1
- Holl, B., Audard, M., Nienartowicz, K., et al. 2018, *A&A*, 618, A30
- Jura, M., Yamamoto, A., & Kleinmann, S. G. 1993, *ApJ*, 413, 298
- Ludwig, H. G. 2006, *A&A*, 445, 661
- Mowlavi, N., Lecoœur-Taïbi, I., Lebzelter, T., et al. 2018, *A&A*, 618, A58
- Tabur, V., Bedding, T. R., Kiss, L. L., et al. 2009, *MNRAS*, 400, 1945
- Whitelock, P. A., Menzies, J. W., Feast, M. W., et al. 2009, *MNRAS*, 394, 795